Estimation of Magnetic Co-Energy in Salient Pole Rotor Type Single Phase SRM

Jun-Ho Kim*, Eun-Woong Lee*, Hyun-Kil Cho*, Jong-Han Lee* and Chung-Won Lee*

Abstract - The salient pole rotor type single phase SRM (switched reluctance motor) uses radial and axial direction magnetic flux simultaneously. Therefore, the output power per unit volume is very high and the shaft length is shorter than other types of SRMs with the same output. Furthermore, it can be manufactured with low cost owing to its simple structure and driving circuit. The prototype was designed using the theory of the traditional rotating machine and 3D FEM analysis. On this paper, the experiment apparatus, which includes the fabricated prototype in previous researches, was fabricated to measure the current and voltage of the prototype. Then the flux linkage, inductance and magnetic co-energy were calculated using the experimental results. Finally, the measured magnetic co-energy was compared with the simulated magnetic co-energy.

Keywords: Flux linkage, inductance, magnetic co-energy, salient pole, single phase SRM.

1. Introduction

The energy density per unit volume of a salient-pole rotor type single phase SRM, which uses the axial and radial direction magnetic flux simultaneously, is higher than that of single phase SRM only using radial direction magnetic flux. Therefore, the axial length and exciting mmf are smaller than other types of single phase SRM with identical output. Also, it is suitable for operation under poor driving conditions and in narrow places that are difficult to perform maintenance [1, 2].

In the previous studies, the prototype model was designed by using the design parameters of three phase SRM and the dynamic equations of a conventional rotating machine [3, 4]. The characteristic of the prototype - flux density distribution, air gap flux density, approximate torque, and so on - were simulated by 3D FEM and the design parameter was corrected using 3D FEM results. After repeating that process, the final design parameters were determined and the prototype was fabricated with these parameters. Also the driving device, which is suitable for the structure and functions of the prototype, was fabricated for experiments dealing with speed/torque characteristics [5, 6].

On this paper, the magnetic flux density and magnetic co-energy according to the rotor position were simulated by 3D FEM. The experiment apparatus was fabricated with the prototype, the driving device, and measurement devices in order to measure the voltage and current of the prototype. The flux linkage waveform was calculated by the experimental results. As well, the inductance and magnetic co-energy waveform were obtained from the flux linkage waveform. Finally, the measured magnetic co-energy was compared with the simulated co-energy in order to confirm the difference between the experimental results and the 3D FEM simulation.

* Dept. of Electrical and Electronic Engineering, Chungnam National University, Korea. (mocross@hanafos.com, ewlee@cnu.ac.kr, cho8794@hanafos.com, onebell@hanmail.net, truetwins@dreamwiz.com)
Received June 12, 2003 ; Accepted March 31 2004

2. Structural Features

The prototype is composed of six rotor and six stator poles. The stator poles are excited by the single phase winding simultaneously. Fig. 1(a) shows the stator and single phase winding. Fig. 1(b) shows the outer rotor with the salient pole.

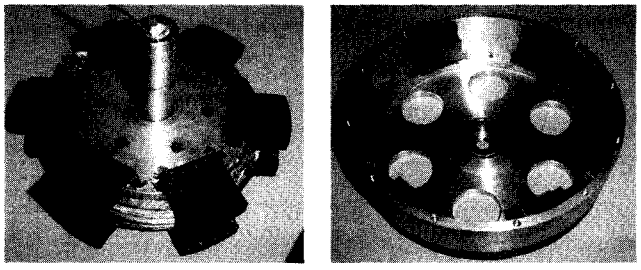

(a) stator and winding (b) outer rotor

Fig. 1 Stator and rotor of the prototype

As shown in Fig. 2(a), the rotor structure with the salient pole uses the axial and radial direction magnetic flux simultaneously. However, the rotor structure without the salient pole such as in Fig. 2(b) only uses the radial

direction magnetic flux. The rotor structure in Fig. 2(a) has a higher flux linkage than the model in Fig. 2(b). Therefore, the prototype, which uses the salient pole in the rotor, has higher energy density per unit volume and can be made shorten the axial length or exciting mmf than other types of SRMs.

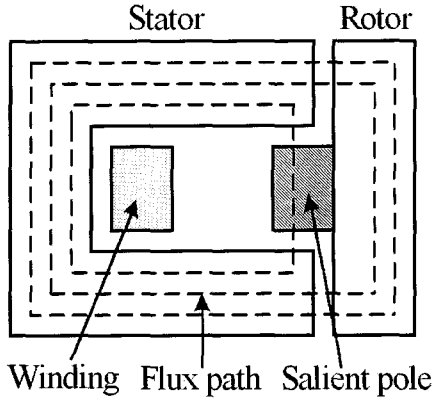

(a) salient pole structure

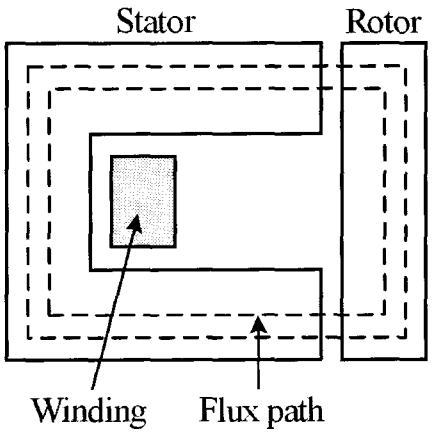

(b) non-salient pole structure

Fig. 2 Rotor structure of prototype

3. Relationship Between Length of Pole Arc And Inductance

3.1 Relationship between length of pole arc and inductance

The conditions of pole arc, which influence the characteristics of the SRM such as the inductance and torque, are shown as equations (1)~(3)[7].

$$\beta_r + \beta_s \leq \frac{2\pi}{N_r} \tag{1}$$

$$\beta_r, \ \beta_s \leq \frac{\pi}{N_r} \tag{2}$$

$$\theta_i = \frac{2\pi}{N_r} \tag{3}$$

where, β_r is the rotor pole arc, β_s is the stator pole arc, θ_i is the periodic angle of inductance variation, N_r is the number of poles.

Equation (1) expresses an inductance variation according to the rotor and stator pole arcs. It is also the condition used to minimize inductance at the unaligned position and can be shown diagrammatically as in Fig. 3(b).

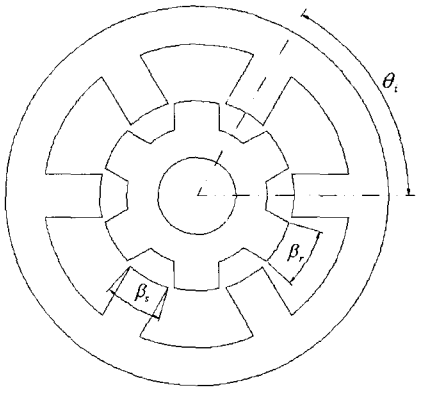

(a) pole arc and period of inductance variation

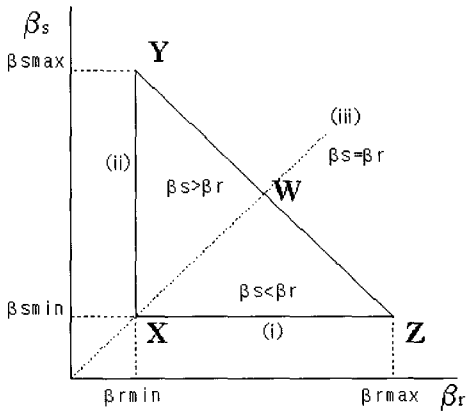

(b) relationship of pole arc

Fig. 3 Relationship between rotor and stator pole arc

There is no maximum inductance zone in the inductance variation at point X because the rotor and stator pole arcs are equal. The stator pole pitch ($2\pi / N_r$) is larger than the length of the rotor and stator pole arcs ($\beta_r + \beta_s$), signifying that the inductance variation has a minimum inductance zone. Therefore, the inductance variation at point X is shown in Fig. 4(a).

As the rotor and stator pole arcs are moved from point X to point Y or Z, the maximum inductance zone is increased and the minimum inductance zone is decreased. At point Y or Z, the maximum and minimum inductance zones do not exist. Fig. 4(b) shows the inductance variation at point Y or Z.

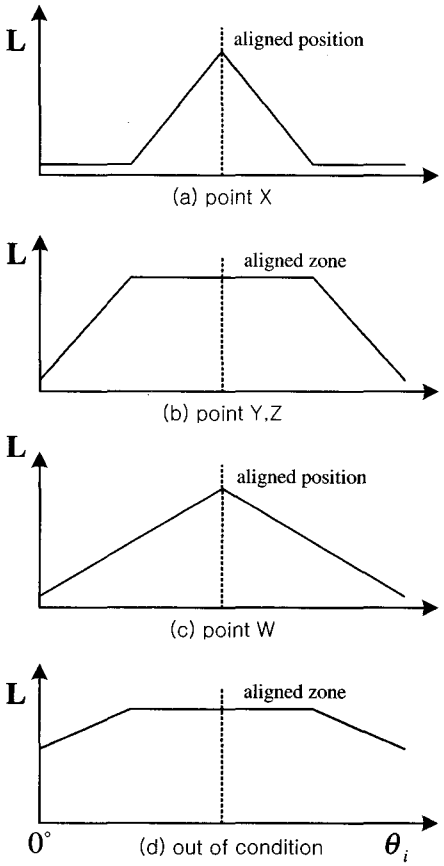

Fig. 4 Inductance variation according to a combination of stator and pole arcs

At point W, the rotor and stator pole arcs are equal. Also, the stator pole pitch is equal to the sum of the rotor and stator pole arcs. Therefore, the maximum inductance zone and minimum inductance zone do not exist at point W as shown in Fig. 4(c). If the lengths of the rotor and stator poles aren't satisfied with equation (1), the minimum inductance becomes very high at the unaligned position as indicated in Fig. 4(d).

If the minimum and maximum inductance zones, which don't generate torque, become larger, the torque zone will be smaller and the output power of the SRM will be also decreased. Therefore, the inductance variation of the general single phase SRM has small minimum and maximum inductance zones similar to that shown in Fig. 4(c).

The increasing or decreasing inductance zones are determined by equation (2). If the rotor and stator pole arcs are increased, the maximum inductance is increased at the aligned position and the increasing inductance area is also increased. But if the rotor and stator pole arcs exceed the condition of equation (2), the stator and rotor poles are overlapped at the unaligned position. Then, the minimum inductance is increased and the torque is decreased. The stator and rotor pole arcs are as large as possible under the satisfying condition of equation (2).

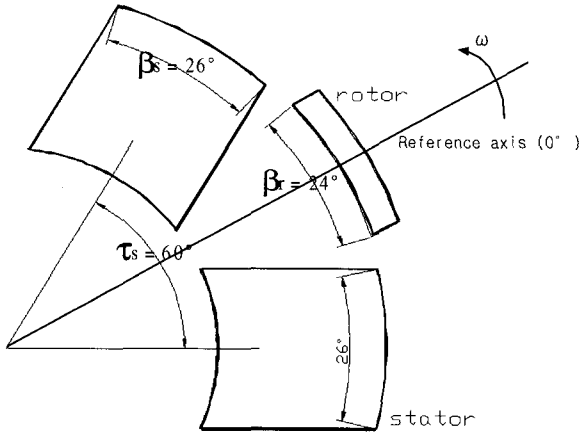

Fig. 5 Rotor and stator pole arcs

3.2 Ideal inductance waveform

The prototype is composed of six stator and six rotor poles. The rotor pole arc is 24 degrees and the stator pole arc is 26 degrees. These poles are placed at intervals of 60 degrees as shown in Fig. 5. Assuming that the position in which the rotor and stator poles begin to overlap is 0 degrees, the inductance variation of the prototype can be represented as in Fig. 6.

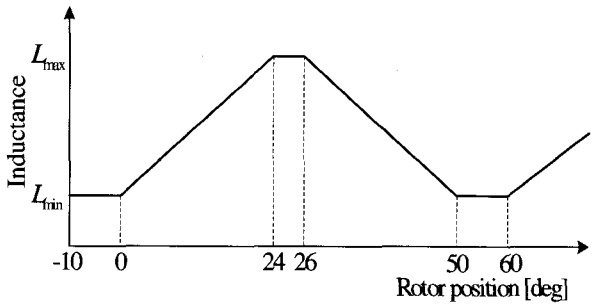

Fig. 6 Ideal inductance waveform of prototype

4. 3D FEM Analysis

4.1 Distribution of magnetic flux density

The distribution of the magnetic flux density at the aligned and unaligned positions was analyzed by the Magnet 6.4 3D FEM program. Each of the following MMFs such as 200[AT], 250[AT] and 300[AT] were applied to the simulation model and each of the magnetic flux densities according to MMF were obtained. Fig. 7 and Fig. 8 show the distribution of the flux density with 300[AT].

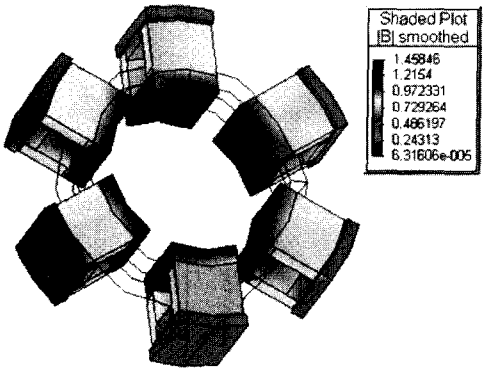

(a) aligned position (300[AT])

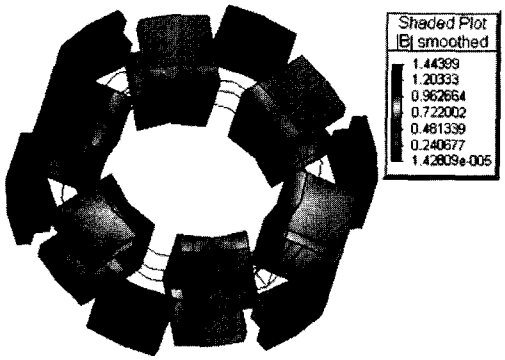

(b) unaligned position (300[AT])

Fig. 7 Distribution of flux density according to rotor position I

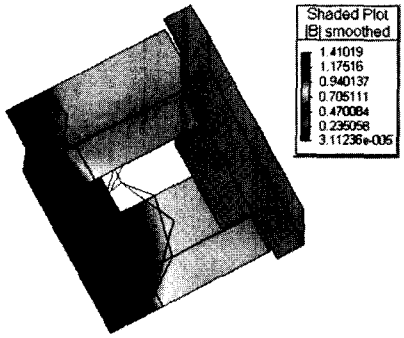

(a) aligned position

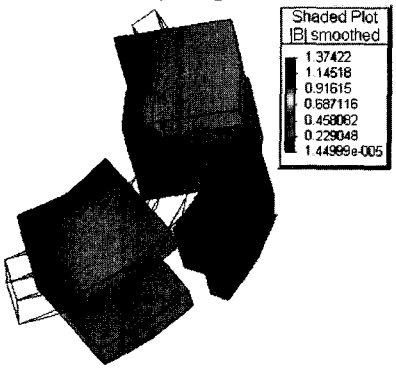

(b) unaligned position

Fig. 8 Distribution of flux density according to rotor position II

4.2 Simulated magnetic co-energy

The magnetic co-energy $W_i(\theta)$ at the aligned and unaligned positions was also obtained by 3D FEM as indicated in Table 1.

Table 1 Magnetic co-energy according to rotor position

W_i, [AT] \ θ		θ = 0°(aligned)	θ = 30°(unaligned)
$W_1(\theta)$	200[AT]	W_1 = 0.162181	W_1 = 0.075935
$W_2(\theta)$	250[AT]	W_2 = 0.243153	W_2 = 0.109036
$W_3(\theta)$	300[AT]	W_3 = 0.337761	W_3 = 0.14769

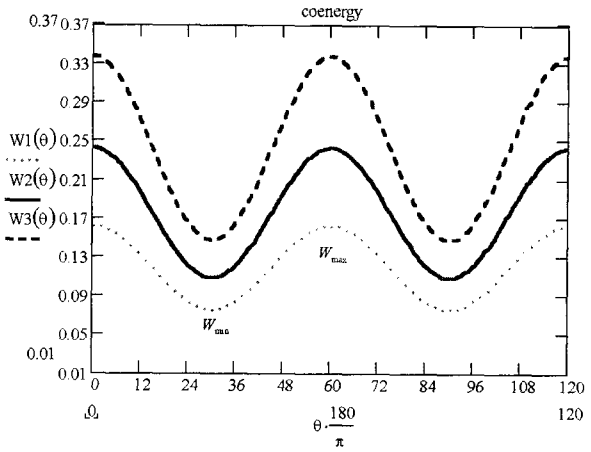

Fig. 9 Calculative co-energy with 3D-FEM

Assuming that the distribution of the magnetic co-energy $W_i(\theta)$ is a sinusoidal waveform from the aligned position to the unaligned position, the distribution of the magnetic co-energy can be approximate as shown in Fig. 9 with equation (4)[9].

$$W(\theta) = W_{avg} + W_p \cos(p\theta) \quad (1)$$

where, $W_{avg} = W_{\min} + W_p$

$$W_p = \frac{W_{\max} - W_{\min}}{2}$$

5. Measurement of Magnetic Co-Energy

5.1 Constitution of measurement device

The experiment apparatus is composed of the prototype, two DC power supplies, a DC motor and measuring equipments as shown in Fig. 10. One of the DC power

supplies excites the prototype, and the other operates the DC motor, which rotates the prototype.

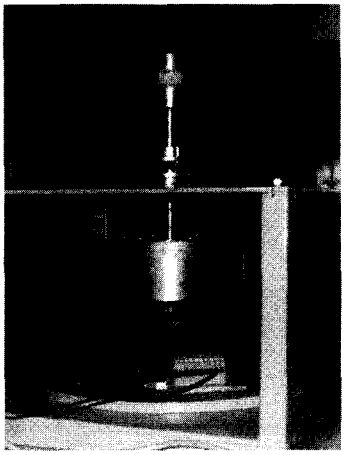

(a) prototype and DC motor

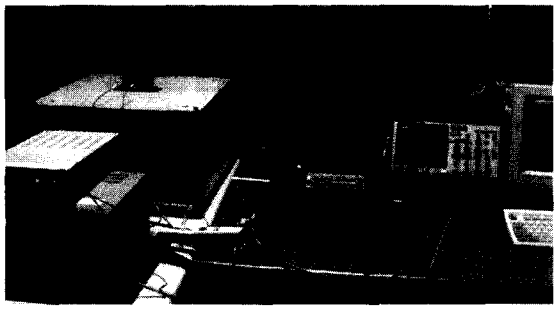

(b) measurement apparatus

Fig. 10 Experiment setup

5.2 Measurement of voltage and current

The prototype was excited by the DC power supply 6[A]. During that time, the prototype was rotated with 180[rpm] by the DC motor installed in the upper side of the experiment apparatus and the voltage v and the current i were measured using measurement systems such as the oscilloscope and GPIB. The exciting winding resistance R was varied by the heat generated in the winding, but the variation of the winding resistance was ignored in this experiment. Therefore, it was measured under the condition in which the prototype was not excited.

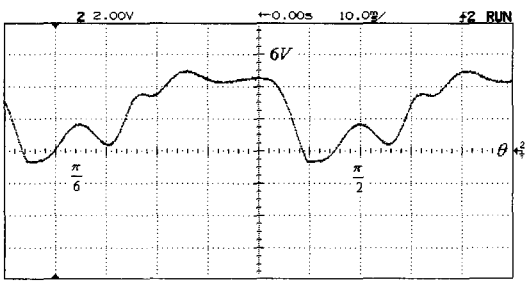

(a) voltage waveform

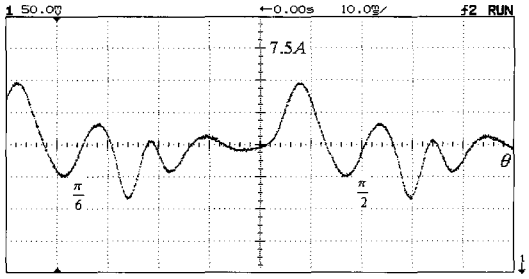

(b) current waveform

Fig. 11 Voltage and current waveform

The current oscillated with ` 1[A] amplitude on the level of 6[A] and the voltage varied more heavily than the current from 5[V] to -0.7[V].

5.3 Measured magnetic co-energy

Equation (5) is the voltage equation of SRM. Equation (6) is derived from integrating equation (5) and rearranging the flux linkage Φ.

$$v = R + \frac{d\Phi}{dt} \tag{5}$$

$$\Phi = \int (v - Ri)dt + \Phi_0 \tag{6}$$

Φ_0 is the initial value of the flux linkage at the start position of the integral. Assuming that the integral in equation (6) is initiated at the unaligned position, Φ_0 is the flux linkage at the unaligned position.

The prototype was applied to the exciting current after the prototype was fixed at the unaligned position. The voltage and current were measured. With these experiment results, the flux linkage waveform according to exciting current was calculated using equation (6). Fig. 12 shows the flux linkage at the unaligned position according to the exciting current and Φ_0 is 0.014048[wb].

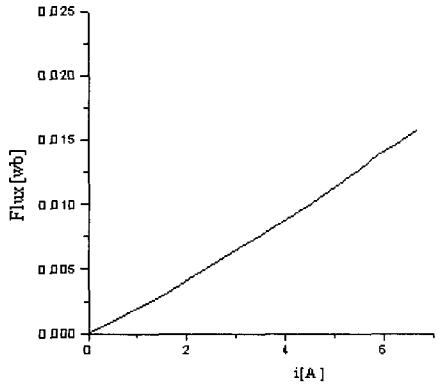

Fig. 12 Flux linkage waveform at unaligned position

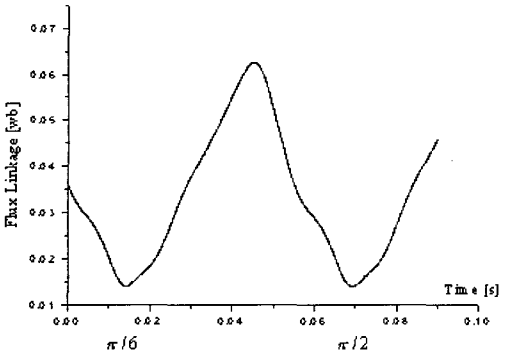

Fig. 13 Flux linkage waveform (300AT)

All of the required parameters for calculating the flux linkage were obtained. Inserting all parameters to equation (6), the flux linkage waveform was calculated as indicated in Fig. 13. As well, the inductance and magnetic co-energy waveform were calculated by inserting the flux linkage to equations (7) and (8). Fig. 14 shows the inductance waveform and Fig. 15 shows the magnetic co-energy waveform of the prototype.

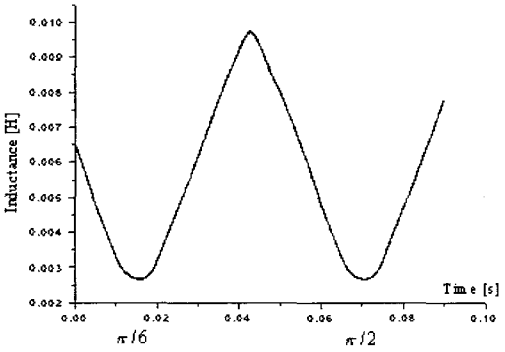

Fig. 14 Inductance waveform (300AT)

$$L = \frac{\Phi}{i} \tag{7}$$

$$W = \frac{1}{2} i^2 L \tag{8}$$

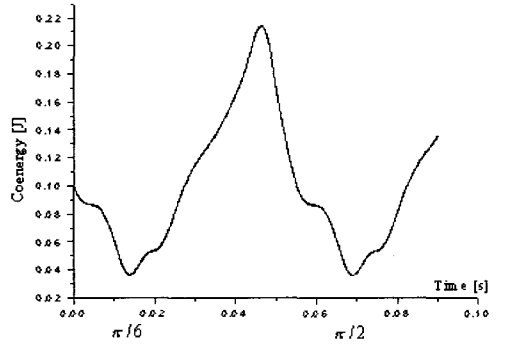

Fig. 15 Co-energy waveform (300AT)

The maximum and minimum inductance zones are 2[degrees] and 10[degrees] respectively in the ideal inductance waveform of the prototype as presented in Fig. 6. In the calculated inductance waveform, the maximum inductance zone is very short and the minimum inductance zone is just as long as in Fig. 6. The flux linkage was increased at the unaligned position because the stator is overlapped with the salient pole.

The exciting winding of the prototype was wound 50 turns and 6[A] current was applied in the experiments. Then, the magneto motive force becomes equal to 300[AT]. This means that the calculated magnetic co-energy waveform corresponds with the 300[AT] waveform in Fig. 9, which is obtained by 3D FEM if there are any losses.

As shown in Table 2, there are significant differences between the calculated magnetic co-energy and the simulated magnetic co-energy. The maximum measured magnetic co-energy is smaller than the simulated magnetic co-energy on 300[AT] and it is similar to 230[AT]. Also, the minimum measured magnetic co-energy is much smaller than the simulated magnetic co-energy. However, the difference of the magnetic co-energy between the aligned and unaligned positions, which affects the torque of the prototype, is in good agreement with the simulated one.

Table 2 Comparison of measured magnetic co-energy and simulated co-energy

[AT] / θ	3D FEM			experiment
	200[AT]	250[AT]	300[AT]	300[AT]
aligned position (max)	0.16	0.24	0.34	0.213
unaligned position (min)	0.07	0.11	0.15	0.035
max - min	0.09	0.13	0.19	0.178

5. Conclusions

The experiment apparatus, which is composed of the prototype, two DC power supplies, a DC motor, and measurement devices, was fabricated to measure the voltage and current of the prototype. The flux linkage, inductance and magnetic co-energy were calculated with the experiment results. The calculated inductance waveform was compared with the ideal inductance waveform. Therefore, it is confirmed that the minimum inductance zone is increased because of the salient pole installed in the rotor.

Furthermore, the magnetic co-energy obtained from the experiments was compared with the simulated magnetic co-energy obtained by 3D FEM. The measured magnetic

co-energy is smaller than the simulated magnetic co-energy. But, the difference of the magnetic co-energy between the aligned and unaligned positions has a good agreement with simulated one.

Acknowledgements

This study was carried out under the supervision of EESRI with the support of KEPCO (NO. 00-042)

References

[1] C.C.Chan, "Single-phase switched reluctance motor", IEE Proc., Vol.134, Pt.B, No.1, pp.53-56, January 1987.
[2] Lee J.H., Lee E.W., Cho H.K, "Fundamental Design of Disk type Single Phase Switched Reluctance Motor", KIEE summer autumn conference, pp.9-11, 1996
[3] Lee J.H., Oh Y.W., Lee E.W., "Manufacturing Prototype and Characteristics Analysis of Disk type Single Phase SRM by 3D Finite Element Method", The Transactions of KIEE, Vol. 48, B, No.6, pp.316-321, 1999
[4] Lee J.H., Lee E.W., Lee D.J., "3D finite element analysis of disk type single phase SRM considering the saturation", e, A, pp.325-327, 1998
[5] Lee J.H., Oh Y.W., Lee E.W., "Manufacturing Driver and Measuring Performance of Disk type Single Phase Switched Reluctance Motor(DSPSRM)", The Trans. of KIEE, Vol.49B, No.1, pp.15-19, 2000
[6] Kim J.H., Lee E.W., Oh Y.W., "Torque measurement of Disk type Single Phase Switched Reluctance Motor", KIEE summer annual conference, B, pp.678-680, 2000
[7] P. J. Lawrenson,, "Variable-speed switched reluctance motor", IEE Proc., Vol.127, Pt.B, No.4, pp.253-265, July 1980.
[8] Cossar, C. and Miller, T.J.E., "Electromagnetic testing of switched reluctance motors", International Conference on Electrical Machines, pp.470-474, September 15-17, 1992
[9] Lee J.H., Lee E.W., Lee D.J., "Approximated Torque Characteristic of DSPSRM by 3D Finite Element Method", KIEE spring annual conference, pp.88-90, 1998.5

Jun-Ho Kim
He received his B.S. and M.S. degrees in Electrical Engineering from Chungnam National University in 1998 and 2002, respectively. He is currently working toward his Ph.D. degree at Chungnam National University.

Eun-Woong Lee
He received his B.S., M.S., and Ph.D. degrees in Electrical Engineering from Hanyang University in 1971, 1974, and 1984, respectively. He is currently a Professor in the Department of Electrical Engineering, Chungnam National University. He worked as a Visiting Faculty in the Department of Electrical Engineering at McGill University from 1982 to 1983 and from 1985 to 1986. He is a member of KIEE and JIEE and a senior member of IEEE. He is interested in several kinds of motors such as LPM, single phase SRM, the wobble motor and the induction motor.

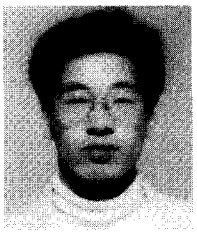

Hyun-Kil Cho
He was born in Korea on June 10, 1969. He received his B.S. and M.S. in Electrical Engineering from Chungnam National University in Daejeon, Korea in 1994 and 1996, respectively. He has been designing magnetic contactors and carrying out an analysis of electromagnetic phenomena for LG Industrial Systems Company in Cheongju, Korea since 1996. He is working toward his Ph.D. degree at Chungnam National University.

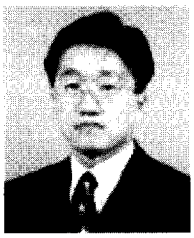

Jong-Han Lee
He received his B.S. and M.S. degrees in Electrical Engineering from Chungnam National University in 1993 and 1999, respectively. He currently works at Chonan Technical High School. He is working toward his Ph.D. at Chungnam National University.

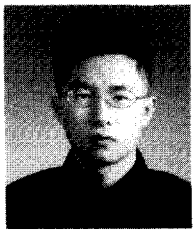

Chung-Won Lee
He received his B.S. degree in Electrical Engineering from Chungnam National University in 2003. He is currently working toward his M.S. degree at Chungnam National University.